UNIVERSITI MALAYSIA PAHANG

ORIGINAL ARTICLE

Characteristics of six layered Al/Si₃N₄ functionally graded materials prepared through two-step pressureless sintering process

M.I.A. Latiff[1], I. Ismail[1] and D.M. Nuruzzaman[2]

[1] Faculty of Manufacturing and Mechatronics Engineering Technology, Universiti Malaysia Pahang, 26600 Pekan, Pahang, Malaysia

[2] College of Engineering and Technology (CEAT), International University of Business Agriculture and Technology (IUBAT), Dhaka, Bangladesh

ABSTRACT – The rapid advancement of the welding technology has simultaneously increased the demand for the online monitoring system in order to control the process. Among the methods that could be possibly used to assess the weld condition, an air-borne acoustic method grasps the attention from scholars due to its ability to provide a simple, non-contact, and low-cost measurement system. However, it is still lack of resources involving this subject in an attempt to deeply understand the emitted sound behaviour during welding especially when dealing with a complete deviation of a process parameter, welding types, workpiece material as well as the noise from the surrounding. This paper reviews the application of the acoustic method in monitoring the welding process. Specifically, this review emphasized the source of both structure-borne and air-borne acoustic during the welding process and the significance of applying the acoustic method in more detail. By focusing on the liquid state welding process, the scope of discussion converged on the arc and laser welding process. In the last part of this review, the potential future advancement of this method is pointed out before the overall conclusion is made.

INTRODUCTION

Metal matrix composites (MMC) which consist of Aluminium (Al) as the matrix phase are classified as Aluminium metal matrix composite (AMMC). AMMCs have become a central attraction for applications as automotive and aerospace materials due to the desirable mechanical and tribological properties like high specific strength, enhanced wear resistance and thermal properties as well as dimensional stability [1]. The AMMCs have an apparent advantage in terms of the economic perspective as Al is less expensive compared to other lightweight structural metals, for example magnesium, Mg and titanium, Ti [2]. The reinforcement phases for AMMC are usually composed of ceramic constituents either in the form of particles [3], fibres [4] or whiskers [2]. AMMC can be tailored into Functionally Graded Materials (FGM) structures comprising of metal and ceramic layers combined through spatial gradation of each constituent's composition. The material gradient in the FGM structures reduced or relaxed the stress jumps near the interfaces and ultimately improved the interfacial bondings [5]. In addition, through FGM the optimum composition of reinforcement can be obtained to minimise the cost of pure ceramics like Si_3N_4 while attaining the desirable properties regionally for better functional performance. Aluminium Silicon Nitride (Al/Si_3N_4) system is a suitable composite material to be produced as functionally graded automotive components for application in engine cylinder liners, piston and brake rotor disc [2].

FGM structures can be produced using various methods, including stir casting and powder metallurgy. Research related to FGMs always deal with achieving desired performances by controlling microstructural properties in the tailored material composition. Compared to the casting technique that produced the continuous gradation due to centrifugal force, the Powder Metallurgy (PM) technique can tailor discrete gradation in FGM for any specimen shapes. The PM technique is reliable to produce pre-designed microstructures and micro-porosities on FGM parts [5]. The sintering process is a significant step in the PM technique because it functions to consolidate the powder-compact PM materials by heating the specimen to a temperature below the constituents' melting point. Sintering can be done either pressureless or pressure-assisted. Hot-press and spark plasma sintering (SPS) are the example of pressure-assisted sintering. However, the pressure-assisted techniques require sophisticated machines associated with high production costs which limit the industrial applicability [1]. Thus, pressureless sintering technique can be an alternative method to overcome those limitations as this technique is proven to produce good FGM properties.

Some approaches to improve the densification and properties of various composites and FGM systems through pressureless sintering process include changing of powder particle sizes and shapes, controlling of process parameters (sintering temperature and time) as well as modifying the sintering profiles. One of the FGM produced using the pressureless sintering process is the alumina–iron (Al_2O_3-Fe) FGM with three-graded layers sandwiched by the pure constituent layers [6]. The fabrication process employed a simple route of die pressing followed by pressureless-sintering in a vacuum furnace at 1400 ℃ for 3 hours. The powder particle sizes of the alumina and iron pure layers were changed from the FGM layer mixtures while the heating rates during sintering process were varied based on temperature. The FGM produced through this approach showed good integration between layers with no crack or delamination. Different powder particle sizes helped to minimize the shrinkage difference between the FGM layers. Microstructural observation

of the Al_2O_3-Fe FGM showed the presence of isolated pores which indicated relatively high-density gradient FGM components (between 88–94 % of theoretical density) [6]. Another study showed that unifrom shrinkage gradient can prevent cracks or delamination in the FGMs. An empirical formulation relating shrinkage and material composition was established and used to minimize shrinkage differences within the FGM parts [7]. Ni-Al_2O_3 FGM configurations comprised of varied number of layers were sintered in a tube furnace at 1350 ℃ and maintained for 3 hours. Consequently, an optimised FGM sample which consisted of nine layers and having uniform shrinkage gradient was produced [7]. It was also reported that the pressureless sintering technique was effective for producing low porosity TZ3Y/Ni FGM and non-graded composites with 95.2 % relative density [8]. The FGM comprised of pure zirconia layer and five composite layers where the metal inclusion (Ni) varied by 10%. The specimens were pressureless sintered at 1400 ℃ for 2 hours under vacuum condition. The high relative densities were attributed to the small initial particle size of zirconia (0.3µm) as well as its high sinterability [8].

In the study of nano-sized Ni/Al_2O_3 composite, it was shown that the densification and hardness were significantly affected by the sintering profile [9]. The Ni/Al_2O_3 composite was sintered for 3 hours at 1350 ℃ following two different H_2 reduction profiles to prevent Ni oxidation. In the first sintering profile, the reduction process was held for 2 hours at 700 ℃ while the second one had the reduction gas flowed through from the room temperture up to 1000 ℃. Results form that study acknowledged that the sintering profiles affected both density and hardness through grain growth promotion or retardant [9]. The use of fiber reinforcement was also proven to be effective for the enhancement of mechanical properties of composites [4]. Aluminium–silicon nitride metal matrix composites with 0.5 vol.% Si_3N_4 fibre powder reinforcement were produced through the powder processing technique and then sintered at 600 ℃ for 1 hour. The hardness results of the Al/Si_3N_4 composite increased significantly to 36 ± 3 HRB compared to the pure Alumix123 hardness of 28 ± 3 HRB. Other study reported that incorporation of nano Hydroxyapatite (HA) resulted in improved densification of HA FGMs with hybrid reinforcement of stainless steel 316L (SS316L) and carbon nanotubes (CNTs) [10]. The FGMs had been synthesised through pressureless sintering at 950 ℃ for 3 hours with three dwell stages of 30 minutes at 120 ℃, 300 ℃ and 550 ℃. Sintering temperatures and sintering times were controlled to prevent formation of cracks in the FGM. The FGM density improvement was attributed to the incorporation of nano-sized HA particles used. However, at high nanoparticles concentrations beyond the maximum packing density, the FGM density declined and led to cracking of samples [10].

Considering the sintering temperature and time, the latter proven to be a more significant factor in terms of hardness improvement. Four-layered aluminium-aluminium oxide (Al/Al_2O_3) FGMs having 0, 10, 20 and 30 by weight percentages of ceramic constituents were prepared through powder metallurgy (PM) route [11]. Consolidation of the powder compacts were done through two-step pressureless sintering profile from room temperature up to 600 ℃ and held for 3 hours. The results showed increasing trend of Vickers microhardness and diameter shrinkage with the increasing of Al_2O_3 percentages. The hardness recorded at the pure Al layer was 29.6 HV while the highest hardness value recorded was 35.2 HV at the 30 wt.% layer [11]. Following the similar procedure and same FGM composition, the FGMs were consolidated at higher temperature (620 ℃) but shorter sintering time (2 hours). As a result, the hardness of the FGM layers showed lower values of 23.81 HV at the pure Al layer and 27.96 HV at the 30 wt.% Al_2O_3 layer [12]. Similar results were also reported for the six-layered Ni-Al_2O_3 FGMs. The FGM layers had linear compositional gradation from pure (100 wt.%) Ni to pure Al_2O_3. The FGMs were sintered via pressureless sintering technique at 1200 ℃ for 3 and 4 hours respectively. For the 3 hours sintering time, the lowest hardness obtained was 12.03 HV while the highest hardness was 150.00 HV [13]. As for the 4 hours-sintered FGM, the lowest hardness recorded was 20.775 HV while the highest hardness recorded was 310.25 HV [3]. However, some layers showed decreasing microhardness due to high porosities as a result of incomplete sintering process.

In addition to the dwelling time at the respective sintering temperature, holding times or steps prior to the sintering time were reported to contribute to the uniform grain shape and reduced porosity [5]. Five-layered Ni/TiO_2 FGM samples were prepared via pressureless sintering and held for 90 minutes at the sintering temperature of 1200℃. The sintering profiles included three steps at every interval of 300 ℃ with the holding times of 15 minutes for each step. The reported densities of the Ni/TiO_2 FGMs showed that the pure metallic layer achieved high densification (91% of theoretical density) and decreasing towards the pure ceramic layer. On the other hand, the hardness results of each layer showed increasing plots with the increase in TiO_2 content from 120 to 225 HV [5]. The effects of dissimilar cooling rates were reported in terms of the densification and hardness [14]. Four variations of FGM's spatial gradations embedded in four graded layers were prepared through powder metallurgy and pressureless sintering techniques. The FGMs were pressureless sintered at 1200 ℃ for 90 minutes followed by cooling at different rates such as 5 ℃/min, 15 ℃/min, 20 ℃/min and 25 ℃/min. The results indicated that higher densities and hardness results were recorded from the FGMs consolidated at higher cooling rates. The cooling rate of 20 ℃/min appeared to produce better microstructural and mechanical properties for the FGMs.

In the light of the previous works, pressureless sintering technique is proven to be a potential method for the fabrication of composites and FGMs with enhanced properties. The study on Al/Si_3N_4 FGM system in particular those prepared through two-step pressureless sintering technique is still scarce and potential to be studied for the applications in high-end FGM products like in the automotive and aerospace industries. The main motivation of this study is to prepare functionally graded Al/Si_3N_4 composites through powder metallurgy and two-step pressureless sintering techniques having increased hardness-property. The samples' characteristics will be determined layer by layer in terms of the microstructures and hardness properties of the FGM.

MATERIALS AND METHODS

Raw Materials

Pure aluminium powders (Tunchem (Shanghai) Pharm Tech. Co. Ltd., (China)) with purity of 99% and average particle size 20 µm were used for the matrix phases, while silicon nitride powders (Si_3N_4, Sigma Aldrich, USA) with nominal size of ≤10 µm were used as the reinforcement phases to synthesise the FGMs. Figure 1 shows the scanning electron microscope (SEM) images of the as-received Al and Si_3N_4 powders, while some properties of the powders are listed in Table 1. The Al particles are spherical in shapes while the Si_3N_4 particles are of acicular shapes formed into clusters.
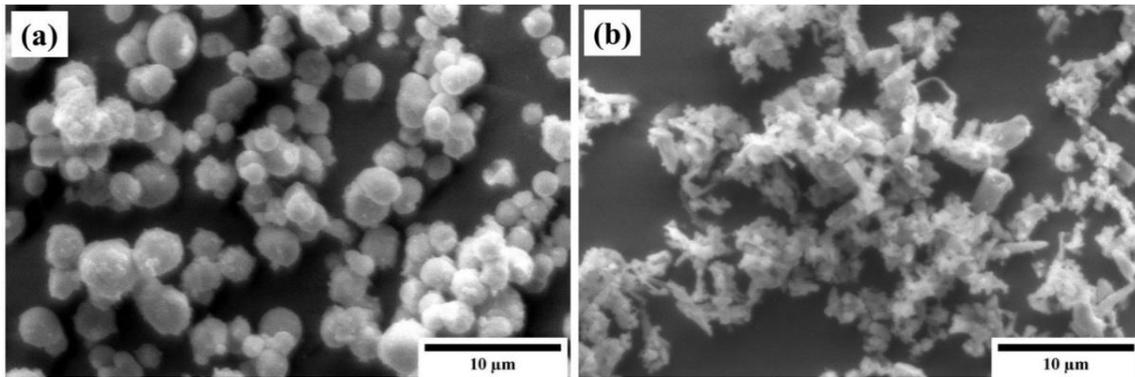

Figure 1. SEM images of raw materials: (a) Al powders and (b) Si_3N_4 powders

Table 1. Properties of aluminium and silicon nitride as-received powders

Constituent PPowders	Molecular weight (g/mol)	Density, at 25 ºC (g/cm³)	Average particle size (µm)
Aluminium, Al	26.982	2.70	20
Silicon nitride, Si_3N_4	140.283	3.44	≤10

Processing

In this study, six layered functionally graded aluminium-silicon nitride (Al/Si_3N_4) samples were prepared via conventional powder processing technique followed by two-step pressureless sintering method [3,8]. The spatial gradation was created by increasing the composition of reinforcement particles (Si_3N_4) by 5 wt.% increment in the Al matrix following the rule of mixture. Firstly, the compositions of Al and Si_3N_4 powder constituents in each FGM layer were determined and weighed accordingly. The calculations were based on the molecular weight percentage (wt.%) of the powder constituents. Table 2 shows the calculation of phase composition for each constituent in the respective layer. It is worth to mention that reinforcement higher than 20% was shown to not bring about further strength to the composites. Rather, the agglomerates will form more easily, which will lead to the presence of voids and cracks. Thus, the final layer mixture of 75 wt.% Al + 25 wt.% Si_3N_4 is added as a controlled layer and experiment to confirm the statement. After that the constituent powders were premixed in separate containers with respect to the layer compositions. The mixed powders were sieved through a 200-micron mesh to pulverise particle agglomerates, and then ground using mortar and pestle to obtain homogeneous mixtures. Next, the powder mixtures were subsequently dried in a vacuum oven at 100 °C for 1 hour. The Al/Si_3N_4 FGM structure was constructed by properly stacking up the powder mixtures layer by layer in a steel die of 30 mm diameter as shown in Figure 2(a). The volumes of powder mixtures for every layer were fixed at 2.50 ml using designated spoon in order to control and maintain the thickness of each layer and the whole FGM samples. The composite layer with 25 wt.% Si_3N_4 was laid first while the pure Al layer was placed near the upper punch. The FGM sample configuration is shown in Figure 2(b). After that the stacked powders were cold-pressed uniaxially at a pressure of 30 ton (414 MPa) using a hydraulic press (TOYO: Model TL30, capacity: 30 tonne).

Table 2. Calculation of phase compositions for each constituent in the respective layer

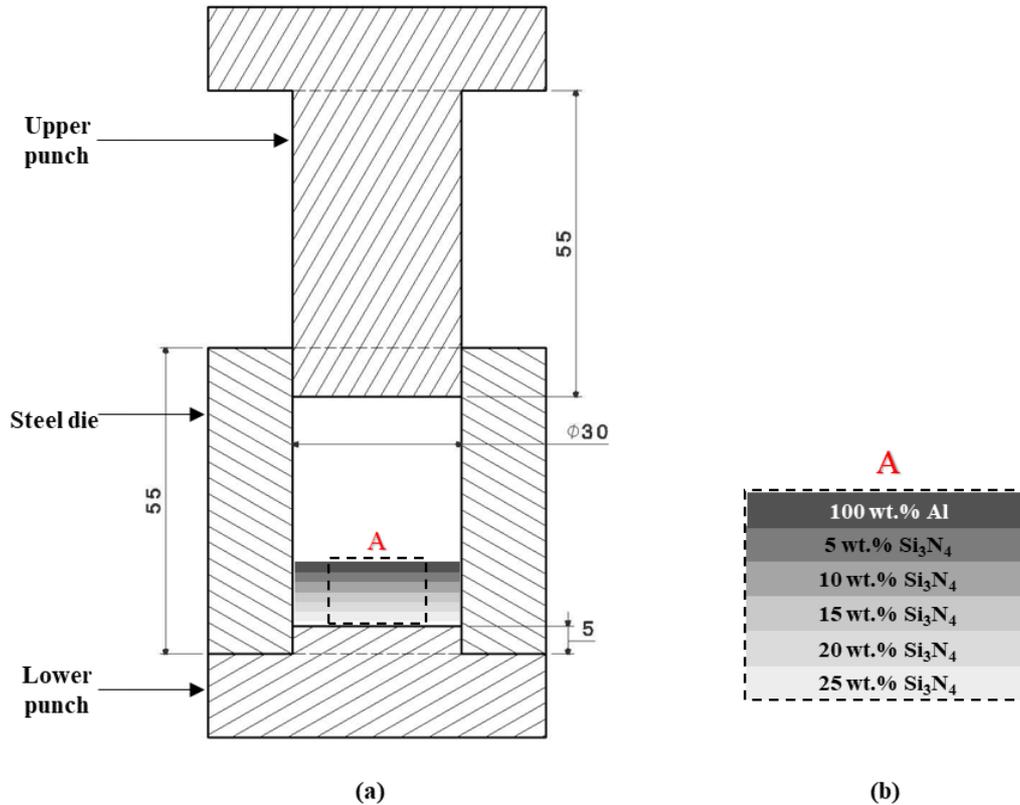| Layer	Layer compositions	Weight of powder constituent (g)	
		Al	Si_3N_4
1	100% Al	26.982	-
2	95 wt.% Al + 5 wt.% Si_3N_4	25.632	7.014
3	90 wt.% Al + 10 wt.% Si_3N_4	24.283	14.028
4	85 wt.% Al + 15 wt.% Si_3N_4	22.934	21.043
5	80 wt.% Al + 20 wt.% Si_3N_4	21.585	28.057
6	75 wt.% Al + 25 wt.% Si_3N_4	20.236	35.071

Figure 2. (a) Schematic diagram of sample preparation and (b) Detail of A (FGM sample configuration)

After compaction, the green compacts were sintered in a pressureless sintering furnace (Nabertherm: made in Germany) following two-step sintering profiles. The samples were heated at a constant rate of 4 °C/min throughout the cycle. The heat treatment was maintained for 30 minutes at 120 °C to allow the evaporation of moistures. After that, heating proceeded to the maximum sintering temperature of 620 °C and maintained for 2 hours. Finally, the samples were cooled in the furnace until the temperature normalised to room temperature. Figure 3 below illustrates the two-step pressureless sintering profile used in this study.

Characterisation

The dimensions of the FGM samples and masses before and after sintering were recorded to determine the volume shrinkage and green density using dimensional method [5]. The sintered density of the FGM samples were measured using Archimedes method with distilled water as the soaking media. The sintered specimens were cut parallel to the thickness direction using an abrasive cutter. Then the cut specimens were cold-mounted on the cross-sectional plane using polymer resin. Afterward, the FGM specimens were ground up to 2000 grit using emery paper and polished using diamond paste. The microstructure and morphology of the sintered Al/Si$_3$N$_4$ FGMs were observed under optical microscope (Olympus model BX51M) followed by scanning electron microscope (SEM, model FEI Quanta 450) for higher magnification images. The SEM was equipped with Electron-dispersive X-ray spectroscope (EDS) to perform the elemental analysis on the samples. The SEM images were analysed using image analysis software (ImageJ 1.53e). Prior to the analysis all images were calibrated with respect to the embedded scales. The microhardness values at each layer in

the FGM samples were measured using Wilson Vickers's microhardness testing machine (Model 402 MVD, made in USA). The measurements were recorded at five different locations for each layer with a minimum distance interval of 1 mm to ensure measurement accuracy and avoid any effect from neighbouring indentations. The indentation load of 300 gf (2.94 N) was applied for dwell time of 15 s [12]. The averages values were reported in this study.
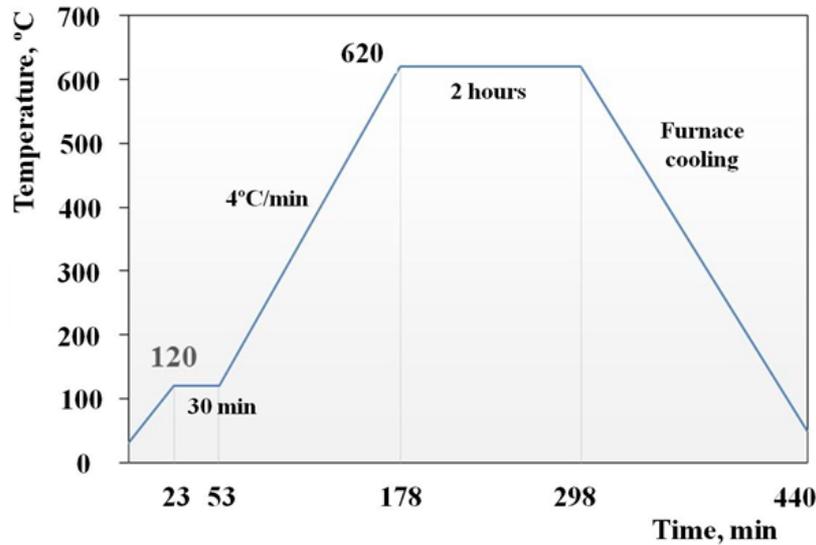

Figure 3. Two-step pressureless sintering profile

RESULTS AND DISCUSSION

Densification and Porosity

The theoretical densities at each layer were calculated using the linear rule of mixture ($\rho = \rho_1 V_1 + \rho_2 V_2$). Then the theoretical density ratios were calculated based on the ratio of powder volume at each layer to the volume of the entire sample. Table 3 below shows the theoretical densities and theoretical density ratios for each layer. The theoratical density ratio for the bulk FGM sample is 2.793 g/cm^3. The measured bulk densities for the green and sintered Al/Si$_3$N$_4$ FGM sample were 1.980 g/cm^3 and 2.549 g/cm^3 respectively, as shown in Figure 4. This implies that the density increased 29% after sintering to achieve a high relative density of 91%.

Table 3. Theoretical density of the 6-layered Al/Si$_3$N$_4$ FGM specimens, calculated using the linear rule of mixture

Al – Si$_3$N$_4$ ratio (%)	Theoretical density (g/cm^3)	Volume (ml)	Theoretical density ratio (g/cm^3)
100 – 0	2.700	2.50	0.450
95 – 5	2.737	2.50	0.456
90 – 10	2.774	2.50	0.462
85 – 15	2.811	2.50	0.469
80 – 20	2.848	2.50	0.475
75 – 15	2.885	2.50	0.481
	Total	15.00	2.793

The porosity (P) of FGM sample was related to the densities by the following Eq. (1) [14]:

$$P = \left[1 - \frac{\rho}{\rho_T}\right] \times 100 \tag{1}$$

where P is the porosity of the sample in percentage, ρ is the green or sintered density and ρ_T is the theoretical density.

The porosity changes between green compact samples and the sintered Al/Si$_3$N$_4$ FGM samples are illustrated in Figure 4. As the density of the sample increased, the porosity in Al/Si$_3$N$_4$ FGM sample was reduced to 8.74% after sintering. The decrease in porosity of the FGM may be attributed to the high sintering temperature of 620 °C as well as uniform dispersion of reinforcement [4].
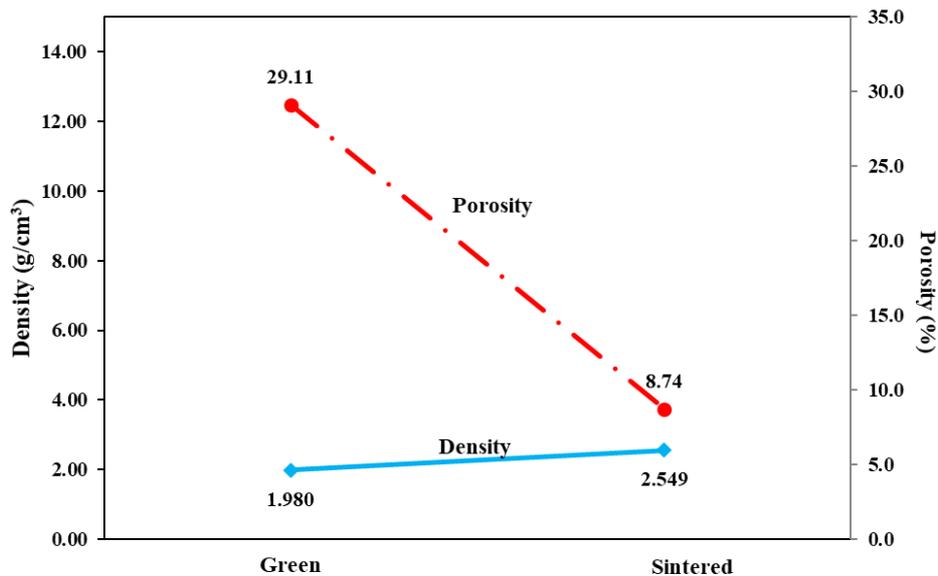
Figure 4. Density and porosity variations between green compacts and sintered samples of Al/Si$_3$N$_4$ FGM samples

Microstructural Characterisation and Composition

Gradient in the functionally graded structures was created by varying the material composition from one end to the other which consequently leads to continuous distribution of the properties. The change of microstructures can be observed in terms of the material compositions and porosities in each respective layer. Figure 5 shows the micrographs from the optical microscopy examinations at every layer in the Al/Si$_3$N$_4$ FGM samples. The metal phases (Al) are identified with the bright parts while the ceramic inclusion (Si$_3$N$_4$) as the dark phases. In the pure Al layer, the dark spots are identified as scratches and pores due to particle pullout from grinding during the sample preparation process. The gradual change in composition could be observed from layer to layer whereby the dark phases increase as the composition of Si$_3$N$_4$ increases. Few Si$_3$N$_4$ agglomerates can be sighted in the 10 wt.% and 15 wt.% Si$_3$N$_4$ layers inherited from the clusters of the as-received ceramic particles. In general, it can be inferred that the distribution of the reinforcing particles were homogeneously distributed in the Al matrix phases.

Figure 6 shows the SEM backscattered images at the layer interfaces of the prepared FGM sample. At higher magnification of the SEM images, the black spots in the micrographs appeared clearly as micro porosities, some of which are pointed by the arrows. As observed in the optical micrographs, the distributions of particles in the SEM micrographs were also uniformly dispersed and no particle agglomerate was sighted. Uniform particle distribution in the matrix is a critical factor that could enhance the hardness property of the FGM [15]. The Si$_3$N$_4$ phases became more dominant from the fourth layer which composition was 15 wt.% Si$_3$N$_4$ up to the sixth layer with 25 wt.% Si$_3$N$_4$ composition. It can be seen that a good integration of the layer interfaces had been achieved, and no crack and delamination was found at the interlayer. Furthermore, most of the porosities observed in the micrographs exist as isolated pores, which is an indication of relatively high density FGM.

The SEM micrographs were investigated further using ImageJ software in terms of the occurrence of porosities in every layer. Figure 7 shows the information on the porosities across the FGM layer with increasing Si$_3$N$_4$ particle content. It is clear that the percentage area of porosities increased with increasing Si$_3$N$_4$ particle content from 0.03% at the pure Al layer to 12.47% in the sixth layer. The increasing of hard reinforcement content in each layer at the same time increased the apparent viscosity of the matrix and consequently the chances of air entrapment. The evolution of adsorbed gases during heat treatment then caused higher porosities with the increase of Si$_3$N$_4$ percentage [16]. Figure 7 also indicates that the average sizes of porosities in every layer are relatively smaller than the Al and Si$_3$N$_4$ particles which are between 1.25 – 2.488 μm.

The SEM images were analysed using EDS to identify the distribution of the elements through elemental mapping. Figure 8 (a) – (l) show the SEM micrographs at different layer interfaces and the respective EDS elemental colour mapping. The blue, red and green colours in the EDS maps represent Al, Si and N, respectively. From the figures, gradual material compositions in the FGM could also be observed whereby the intensities of the blue colour were reducing from layer to layer, indicating the decreasing of Al contents. In contrast, the intensities of the red colours gradually increased which signify the increment of the Si compositions across the thickness direction. Also, it can be perceived from the micrographs that the distributions of all elements were uniformly dispersed.
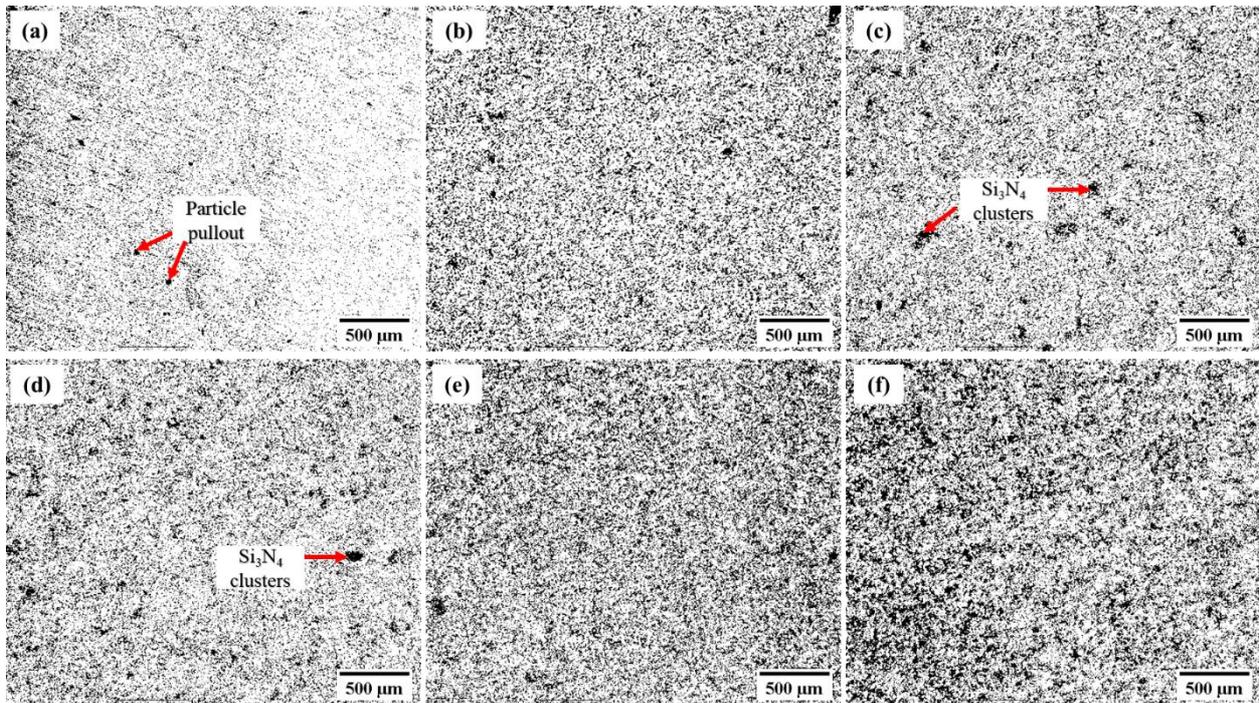
Figure 5. Optical microscope images at the layer interfaces of the prepared FGM sample: (a) 100 wt.% Al, (b) 5 wt.% Si$_3$N$_4$, (c) 10 wt.% Si$_3$N$_4$, (d) 15 wt.% Si$_3$N$_4$, (e) 20 wt.% Si$_3$N$_4$ and (f) 25 wt.% Si$_3$N$_4$
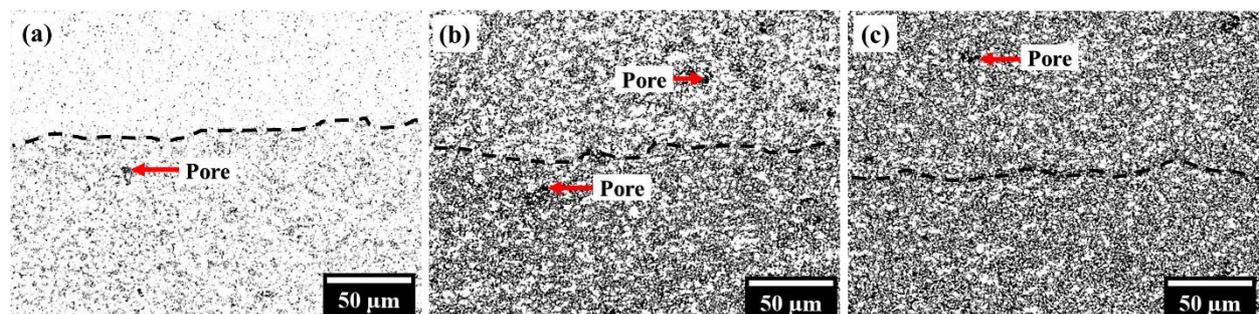

Figure 6. SEM backscattered images at the layer interfaces of the prepared FGM sample: (a) 100 wt.% Al and 5 wt.% Si$_3$N$_4$, (b) 10 wt.% Si$_3$N$_4$ and 15 wt.% Si$_3$N$_4$ and (c) 20 wt.% Si$_3$N$_4$ and 25 wt.% Si$_3$N$_4$

Microhardness Property

Hardness is a representative material property for other mechanical properties. It directly affects the toughness and strength, besides can be a good indication for the estimation of the wear resistance of the material [4]. Figure 9 shows the distribution of Vickers microhardness results along the thickness of Al/Si$_3$N$_4$ FGM sample. The hardness at 100 wt.% Al layer was 68.86 HV and steadily increased with the increase in the Si$_3$N$_4$ content. The increasing trend of hardness values from layer to layer was expected due to the addition of hard ceramic materials into soft and ductile aluminium metallic phase. The increment of hard Si$_3$N$_4$ particles in Al matrix eventually increased the surface area of the reinforcement in the matrix phase. At the same time, growth of Al particles became more restricted thus reduced the size of Al matrix grains. The hard surface areas in the matrix consequently promoted greater resistance towards penetration and plastic deformation of the FGM layers which become the main reason for the improved hardness. The addition of hard Si$_3$N$_4$ particles also at the same time brought about the reduced ductility of the Al matrix, which considerably enhanced the hardness of FGM layer. On the other hand, internal stresses that were inherited from the heat treatment process also contributed towards the improved hardness. Different thermal expansion coefficients between matrix and reinforcement particles lead towards the increase in dislocation density during the solidification process due to the internal stress from plastic deformation of the Al matrix to lodge smaller volume expansion of reinforcement particles. As the reinforcement content increased, the internal stresses augmented the dislocation density at the particle–matrix interfaces causing higher resistance to plastic deformation and ultimately improved hardness [17]. The maximum hardness was recorded at the 20 wt.% Si$_3$N$_4$ layer (205.40 HV), which implies an increment in hardness nearly 200% from the pure aluminium layer.
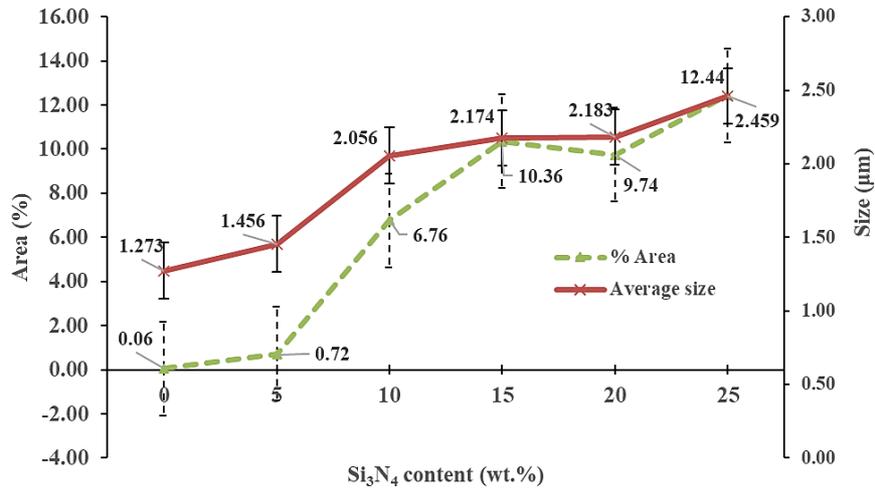
Figure 7. Porosities in the Al/Si$_3$N$_4$ FGM sample analyzed from the SEM micrographs

The hardness results also showed that at the sixth layer whose Si$_3$N$_4$ content was 25 wt.% the value decreased drastically to 53.68 HV. The reason for the hardness drop may be due to the formation of agglomerates and will lead to the occurrence of voids and cracks. Furthermore, excessive reinforcement of particles may affect towards poor densification of composite layer at higher reinforcement content thus do not bring about further strengthening. The results showed similar trend with the reported ultimate tensile strength results from Zhang et al. [15] where the UTS values for Al matrix composites reinforced with β-Si$_3$N$_4$ whiskers recorded increasing magnitudes from 5 vol.% up to 20 vol.% b-Si$_3$N$_4$w addition. However, the UTS occurred at lower values for composite with 30 vol.% β-Si$_3$N$_4$w content, even lower than the Al matrix sintered at temperatures of 530 °C and 550 °C. Figure 10 below shows the microhardness testing images of Al/Si$_3$N$_4$ FGM sample at 100 wt.% Al, 80 wt.% Al and 75 wt.% Al layers, respectively. It can be seen from the figures (a) and (b) that the edges of the indentation marks were vivid while for Figure 10 (c) the indentation was not very clear on the edge because of poor densification of the composite layer. Comparing with the Vickers microhardness results of β-Si$_3$N$_4$w/Al composites reported in Zhang et al. [2], for the same composition, hardness results recorded in this study is 117% higher for the 20 wt.% Si$_3$N$_4$ composition. The β-Si$_3$N$_4$w/Al composites produced in that study was prepared by hot pressing technique with sintering temperature of 560 °C for 2 hours in argon atmosphere.
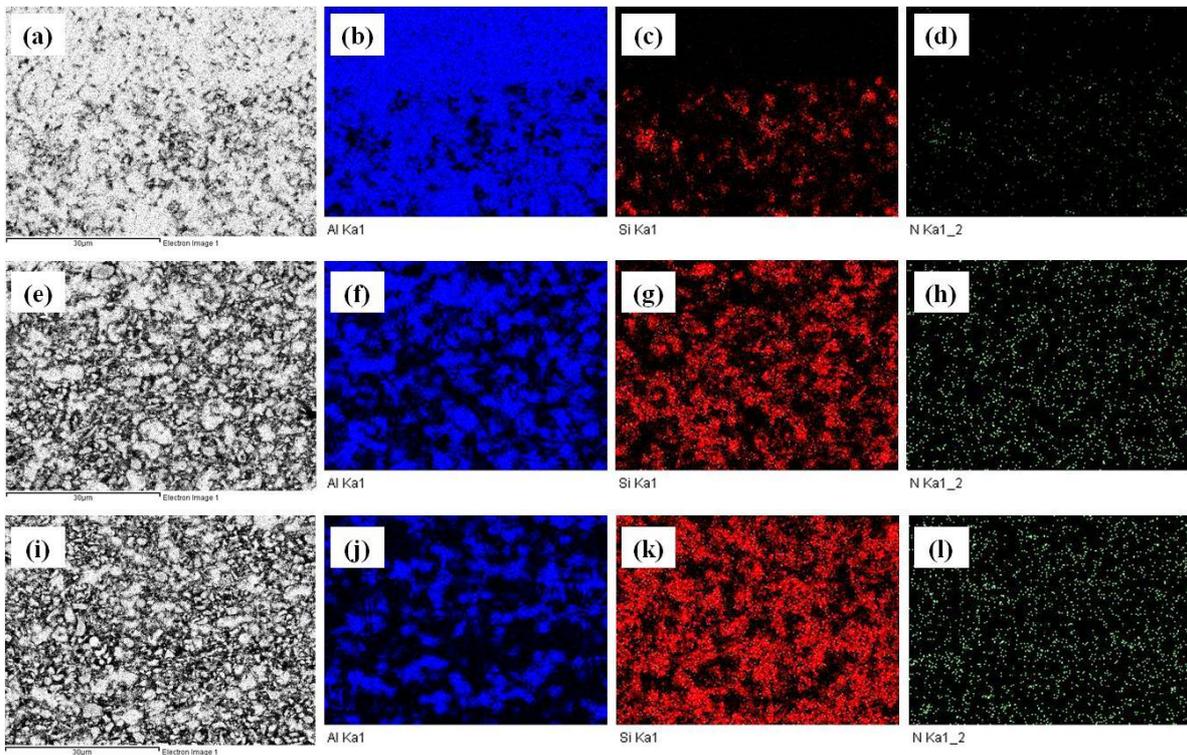

Figure 8. SEM micrographs and respective EDS elemental mapping (Al, Si and N) at the interlayers of: (a)-(d) 100 wt.% Al and 5 wt.% Si$_3$N$_4$, (e)-(g) 10 wt.% Si$_3$N$_4$ and 15 wt.% Si$_3$N$_4$ and (h)-(k) 20 wt.% Si$_3$N$_4$ and 25 wt.% Si$_3$N$_4$
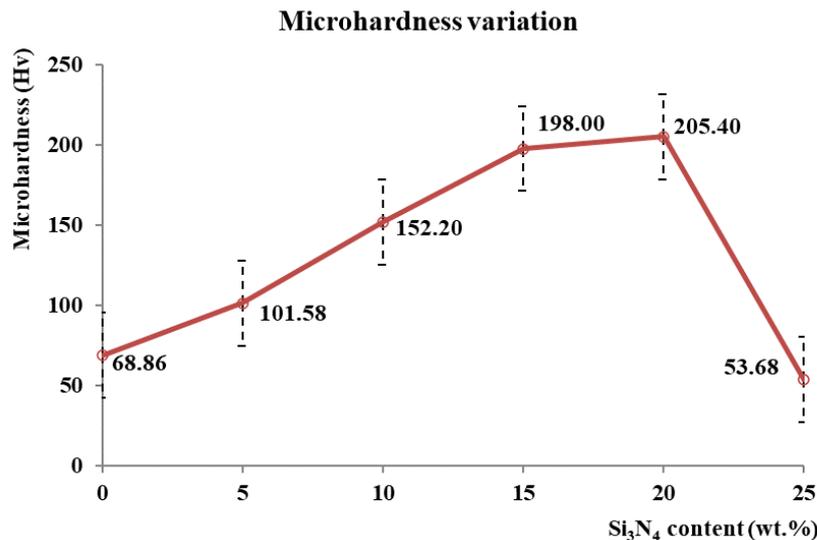
Microhardness variation

Figure 9. Distribution of Vickers microhardness along the thickness of Al/Si$_3$N$_4$ FGM sample
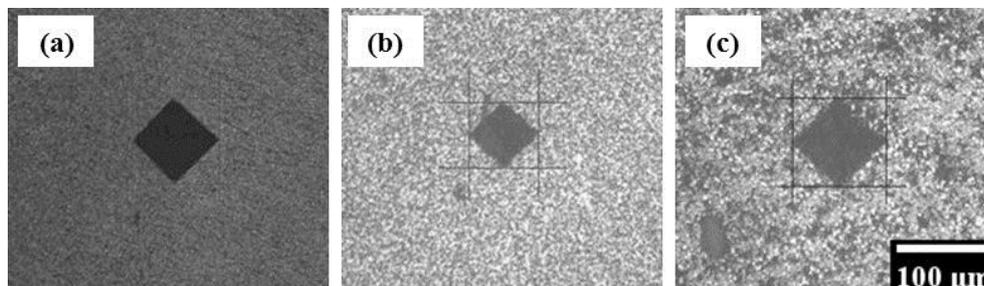

Figure 10. Microhardness testing images of Al/Si$_3$N$_4$ FGM sample at: (a) 100 wt.% Al, (b) 80 wt.% Al and (c) 75 wt.% Al layers

CONCLUSIONS

In this study, six-layered functionally graded Al/Si$_3$N$_4$ composite samples were fabricated through powder metallurgy technique followed by two-step pressureless sintering process. Higher sintering temperature compared to other studies was applied for the densification to take place. The graded layer of the FGMs composed of pure Al layer and consecutive composite layers with 5, 10, 15, 20 and 25 wt.% Si$_3$N$_4$ composition. The SEM micrographs showed that the Si$_3$N$_4$ particles were uniformly scattered in the Al matrix with no agglomeration sighted. The Vickers microhardness results exhibited increasing trend as the hard Si$_3$N$_4$ content was augmented from 5 wt.% up to 20 wt.%. At 25 wt.% Si$_3$N$_4$ inclusion however, the degree of microhardness dropped due to the formation of agglomerates and poor layer densification. The powder metallurgy and two-step pressureless sintering methods proven to be a simple and potential process to fabricate functionally graded Al/Si$_3$N$_4$ composite with high hardness. It can be concluded that for the preparation of Al/Si$_3$N$_4$ FGMs through these procedures, the maximum composition of ceramic powders that could be incorporated is 20 wt.%. Excessive reinforcement content may result towards the formation of agglomerates which will favour the occurrences of voids and cracks.

ACKNOWLEDGMENTS

REFERENCES

[1]   P. Sharma, S. Sharma, and D. Khanduja, "Production and some properties of Si3N4 reinforced aluminium alloy composites," *J. Asian Ceram. Soc.*, vol. 3, no. 3, pp. 352–359, 2015, doi: 10.1016/j.jascer.2015.07.002.

[2]   C. Zhang *et al.*, "Effects of β-Si3N4 whiskers addition on mechanical properties and tribological behaviors of Al matrix composites," *Wear*, vol. 430–431, no. 16, pp. 145–156, 2019, doi: 10.1016/j.wear.2019.05.003.

[3]   S. N. S. Jamaludin, M. I. A. Latiff, D. M. Nuruzzaman, N. M. Ismail, and S. Basri, "Investigation on microstructure and hardness of nickel-alumina functionally graded material," *Mater. Today Proc.*, vol. 29, no. 26, pp. 127–132, 2020, doi: 10.1016/j.matpr.2020.05.644.

[4]   T. Dougherty and Y. Xu, "Properties and characterization of an aluminium–silicon nitride fibre powder metal composite," *SN Appl. Sci.*, vol. 1, no. 135, 2019, doi: 10.1007/s42452-018-0147-z.

[5]   K. A. Bhaskararao and G. R. Janardhana, "Experimental study on mechanical properties of Ni/TiO2 FGM processed by pressureless sintering technique," *Sadhana - Acad. Proc. Eng. Sci.*, vol. 45, no. 1, 2020, doi: 10.1007/s12046-020-01391-5.

[6]   Z. He, J. Ma, and G. E. B. Tan, "Fabrication and characteristics of alumina–iron functionally graded materials," *J. Alloys Compd.*, vol. 486, pp. 815–818, 2009, doi: 10.1016/j.jallcom.2009.07.073.

[7]   S. Yang, H. Kim, and C. S. Lee, "Investigation of shrinkage control in Ni-Al2O3 (Metal-Ceramic) functionally graded materials," *Ceram. Int.*, vol. 39, pp. 93–99, 2013, doi: 10.1016/j.ceramint.2012.05.100.

[8]   M. S. El-Wazery, A. R. El-Desouky, O. A. Hamed, N. A. Mansour, and A. A. Hassan, "Preparation and mechanical properties of Zirconia/Nickel functionally graded materials," *Arab J. Nucl. Sci. Appl.*, vol. 45, no. 2, pp. 435–446, 2012.

[9]   D.-G. Cho, S.-K. Yang, J.-C. Yun, H.-S. Kim, J.-S. Lee, and C. S. Lee, "Effect of sintering profile on densification of nano-sized Ni/Al2O3 composite," *Compos. Part B Eng.*, vol. 45, no. 1, pp. 159–164, 2013, doi: 10.1016/j.compositesb.2012.07.054.

[10]   M. A. Hussain *et al.*, "Improved sinterability of hydroxyapatite functionally graded materials strengthened with SS316L and CNTs fabricated by pressureless sintering," *Ceram. Int.*, vol. 41, no. 8, pp. 10125–10132, 2015, doi: 10.1016/j.ceramint.2015.04.110.

[11]   F. F. Kamaruzaman, D. M. Nuruzzaman, N. M. Ismail, Z. Hamedon, A. K. M. A. Iqbal, and A. Azhari, "Microstructure and properties of aluminium-aluminium oxide graded composite materials," *IOP Conf. Ser. Mater. Sci. Eng.*, vol. 319, no. 012046, pp. 1–6, 2018, doi: 10.1088/1757-899X/319/1/012046.

[12]   F. F. Kamaruzaman, D. M. Nuruzzaman, M. A. Chowdhury, S. N. S. Jamaludin, S. Basri, and Noor Mazni Ismail, "Characterisation of four-layered Al-Al2O3 functionally graded material prepared through powder metallurgy and pressureless sintering," *Int. J. Mater. Prod. Technol.*, vol. 59, no. 1, pp. 48–62, 2019.

[13]   M. I. A. Latiff, D. M. Nuruzzaman, S. Basri, N. M. Ismail, S. N. S. Jamaludin, and F. F. Kamaruzaman, "Preparation and characterization of 6-layered functionally graded nickel-alumina (Ni-Al2O3) composites," *IOP Conf. Ser. Mater. Sci. Eng.*, vol. 342, 2018, doi: 10.1088/1757-899X/342/1/012063.

[14]   K. A. Bhaskararao and G. R. Janardhana, "Microstructure, hardness and flexural strength of Ni/Al2O3 FGMs by pressureless sintering with different cooling rates," *Boletín la Soc. Española Cerámica y Vidr.*, vol. 60, no. 4, pp. 255–265, 2020, doi: 10.1016/j.bsecv.2020.03.012.

[15]   C. Zhang *et al.*, "Enhanced tensile properties of Al matrix composites reinforced with b-Si3N4 whiskers," *Compos. Part A*, vol. 102, pp. 145–153, 2017, doi: 10.1016/j.compositesa.2017.07.025.

[16]   M. Bhattacharyya, A. N. Kumar, and S. Kapuria, "Synthesis and characterization of Al/SiC and Ni/Al2O3 functionally graded materials," *Mater. Sci. Eng. A*, vol. 487, no. 1–2, pp. 524–535, Jul. 2008, doi: 10.1016/j.msea.2007.10.040.

[17]   P. S. Raghavendra Rao and C. B. Mohan, "Study on mechanical performance of silicon nitride reinforced aluminium metal matrix composites," *Mater. Today Proc.*, vol. 33, no. 110, pp. 5534–5538, 2020, doi: 10.1016/j.matpr.2020.03.495.